Atomic layer deposition of titanium nitride for quantum circuits

Abigail Shearrow, Gerwin Koolstra, Samuel J. Whiteley, Nathan Earnest, Peter S. Barry, F. Joseph Heremans, David D. Awschalom, Erik Shirokoff, and David I. Schuster

Citation: Appl. Phys. Lett. **113**, 212601 (2018); doi: 10.1063/1.5053461
View online: https://doi.org/10.1063/1.5053461
View Table of Contents: http://aip.scitation.org/toc/apl/113/21
Published by the American Institute of Physics

Atomic layer deposition of titanium nitride for quantum circuits

Abigail Shearrow,[1,2] Gerwin Koolstra,[1,2] Samuel J. Whiteley,[2,3] Nathan Earnest,[1,2] Peter S. Barry,[4] F. Joseph Heremans,[5] David D. Awschalom,[3,5] Erik Shirokoff,[4] and David I. Schuster[1,2,a)]

[1]*James Franck Institute, University of Chicago, Chicago, Illinois 60637, USA*
[2]*Department of Physics, University of Chicago, Chicago, Illinois 60637, USA*
[3]*Institute for Molecular Engineering, University of Chicago, Chicago, Illinois 60637, USA*
[4]*Department of Astronomy and Astrophysics, University of Chicago, Chicago, Illinois 60637, USA*
[5]*Institute for Molecular Engineering and Materials Science Division, Argonne National Laboratory, Lemont, Illinois 60439, USA*

(Received 23 August 2018; accepted 2 October 2018; published online 19 November 2018)

Superconducting thin films with high intrinsic kinetic inductance are of great importance for photon detectors, achieving strong coupling in hybrid systems, and protected qubits. We report on the performance of titanium nitride resonators, patterned on thin films (9–110 nm) grown by atomic layer deposition, with sheet inductances of up to 234 pH/□. For films thicker than 14 nm, quality factors measured in the quantum regime range from 0.2 to 1.0×10^6 and are likely limited by dielectric two-level systems. Additionally, we show characteristic impedances up to 28 kΩ, with no significant degradation of the internal quality factor as the impedance increases. These high impedances correspond to an increased single photon coupling strength of 24 times compared to a 50 Ω resonator, transformative for hybrid quantum systems and quantum sensing. *Published by AIP Publishing.*
https://doi.org/10.1063/1.5053461

In a superconductor, kinetic inductance (KI) is the inductance due to the inertia of cooper pairs. Films with large KI are attractive for a wide range of superconducting device applications, including high frequency single photon detectors.[1] In addition, the degree of non-linearity of the KI with applied DC current opens up the possibility of novel devices such as superconducting phase shifters,[2] ultra-sensitive current sensors,[3] and quantum-limited travelling-wave parametric amplifiers.[4] Recently, high KI materials have also shown great promise in hybrid quantum systems that aim to couple microwave photons to spin degrees of freedom.[5,6] These materials offer increased spin-photon coupling due to larger zero-point fluctuations of the electric field.[7] The same films can also be used to create superinductors in protected qubit devices.[8–10] Although superinductors have been realized with a chain of Josephson junctions,[11–13] a high KI nanowire is simpler to fabricate, does not suffer from spurious junction modes, and may even provide larger total inductance.[14]

In the thin film limit of superconductivity, KI scales as λ_L^2/t, where t is the film thickness and λ_L is the London penetration depth. Titanium nitride (TiN) is one of the highest known KI materials, primarily due to its large intrinsic London penetration depth, and the KI can be further increased by using ultra-thin films. Microwave resonators fabricated from thin TiN films have exhibited excellent coherence,[15–17] with the highest single photon power internal quality factor exceeding 2×10^6 achieved using sputtering.[18–20] To grow wafer-scale, thin films with consistently high KI, it is important to have uniform film properties across the wafer. Atomic layer deposition (ALD) offers a conformal and repeatable film of TiN and is therefore a promising method for fabricating consistent, high KI microwave resonators. There have been attempts to grow TiN films using ALD,[21,22] and these superconducting films have been used to study deviations from BCS theory.[23]

In this work, we study high KI microwave resonators fabricated from 9 nm to 110 nm thick TiN films that are grown via ALD. Our lumped element resonator design allows for very high characteristic impedance, while maintaining a high coherence. Through a combination of the deposition method, resonator designs, and fabrication procedure, we achieve high internal quality factors (Q_i) exceeding one million at single photon powers for resonators on thicker TiN films. On the thinnest film, we achieve a characteristic impedance up to 28 kΩ, while also reaching $Q_i \approx 10^5$.

In order to understand the film quality of TiN films grown by ALD, we perform materials characterization by DC electrical measurements and X-ray techniques. The superconducting TiN films used in this work are grown on hydrogen-terminated, high resistivity (>10 kΩ cm) Si (111)-oriented substrates, which are cleaned with organic solvents, Nano-Strip, and buffered-HF immediately prior to TiN deposition. During ALD, the substrate is kept at 270 °C, and we use Tetrakis(Dimethylamino)Titanium (TDMAT) and nitrogen gas (N_2) precursors. Each ALD cycle deposits approximately 0.9 Å of TiN, allowing for precise control over the film thickness across the entire wafer. We find that the resulting TiN surface roughness (root-mean-square) is 0.4 nm, measured by atomic force microscopy. After deposition, samples are patterned using standard optical or electron-beam lithography methods and etched using an inductively coupled plasma with Cl_2, BCl_3, and Ar gas flow. Since etch chemistry is known to affect a film's electrical and microwave properties,[19] future work may study the effects of a fluorine-based etch chemistry. We then record the critical temperature (T_c) and sheet inductance ($L_\square$) for a range of different film thicknesses [Fig. 1(a) and Table I]. The inset

a)David.Schuster@uchicago.edu

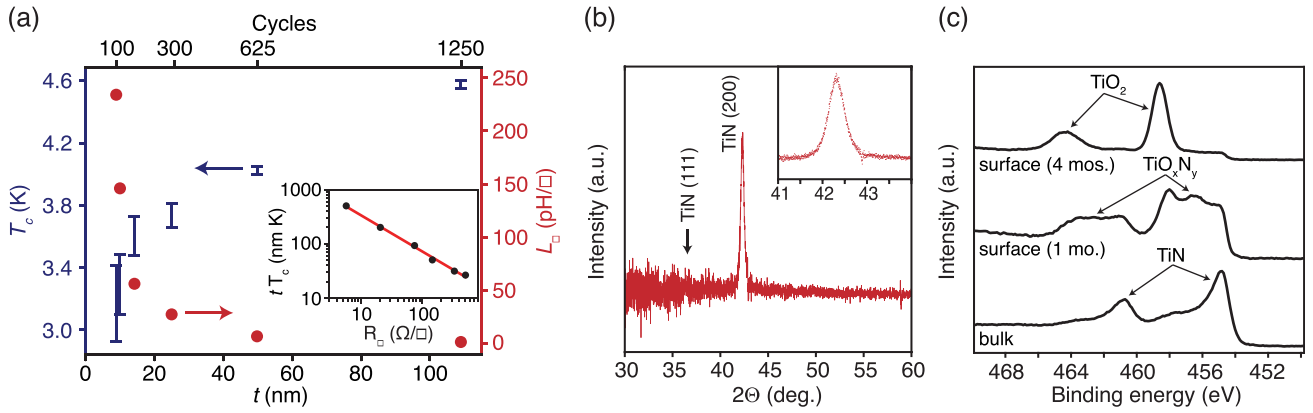

FIG. 1. Materials characterization of TiN grown by ALD. (a) Superconducting critical temperature (T_c) and sheet inductance ($L_\square$) of TiN as a function of film thickness (t). The bars denote the temperatures when there are 10% and 90% reductions in resistivity from the value at 6 K. The inset shows the dependence of tT_c on $R_\square$, with a fit (red line) to $tT_c = A\,R_\square^B$: $A = 1554 \pm 1$, $B = 0.67 \pm 0.02$. (b) $\Theta - 2\Theta$ X-ray diffraction scan of TiN on Si (111). Data are background subtracted using a measurement of the clean Si substrate. The increased noise at lower 2Θ values is from the Si (111) Bragg diffraction peak. (c) X-ray photoelectron spectroscopy of Ti_{2p} surveys from TiN films. Bulk TiN spectra were obtained by Ar^+ ion etching into the middle of a 109 nm thick TiN film. These samples were left in air at room temperature for 1–4 months.

of Fig. 1(a) shows that our films follow a universal relation that links thickness, T_c, and sheet resistance, which has been observed for other thin superconducting films.[24] Moreover, the exponent $B = 0.67 \pm 0.02$ we measure is similar to TiN from other work.[25]

The critical temperature decreases from 4.6 K for the thickest film ($t = 109$ nm) to 3.0 K for the thinnest film ($t = 8.9$ nm), which can be attributed to disorder enhanced Coulomb repulsions.[23,26] It is worth mentioning that we were unable to produce a superconducting film with $t \approx 5$ nm (Fig. S1). Nevertheless, TiN grown by ALD thinner than $t = 8.9$ nm has been shown to go superconducting,[21,23] and it is possible that more optimization of surface preparation and the growth recipe could allow for thinner superconducting films by this method.

A main feature of these films is their high kinetic inductance. We determine this quantity from $L_\square = \hbar R_\square / \pi \Delta_0$, where the sheet resistance $R_\square = \rho/t$ is measured just above T_c and $\Delta_0 = 1.76 k_B T_c$ is the superconducting energy gap for TiN[26,27] predicted by BCS theory. A monotonic decrease in T_c with the decreasing film thickness is therefore linked to a monotonic increase in $L_\square$, which is eventually limited by the thinnest film we can grow that still superconducts. We achieve a maximum $L_\square = 234$ pH/□, more than a hundred-fold increase compared to the thickest film. This demonstrates the potential for TiN grown via ALD as a high KI material.

TABLE I. Properties of ALD TiN films for various thicknesses. The thickness (t) of each film is measured via ellipsometry, except for thicknesses marked with an asterisk (*), which are interpolated. The remaining parameters are determined from four wire resistance measurements. The critical temperature (T_c) shown is the temperature at a 50% reduction in resistivity (ρ) from 6 K.

Cycles	t (nm)	T_c (K)	ρ ($\mu\Omega$ cm)	$L_\square$(pH/□)
100	8.9	3.01	449	234
125	10.7*	3.17	332	146
187	14.2	3.63	206	56
300	25.7*	3.76	186	28
625	49.8	4.05	103	7.1
1250	109.0	4.62	62	1.7

We perform X-ray diffraction to determine the dominant crystal orientation of the films. The X-ray diffraction patterns of a 109 nm thick TiN sample, chosen in order to yield the highest intensity, show a Gaussian peak at $2\Theta = 42.32° \pm 0.01°$ [Fig. 1(b)], corresponding to (200)-oriented TiN. Furthermore, there is no detectable diffraction peak from (111)-oriented TiN at $2\Theta \approx 36.5°$. We estimate a lattice parameter $a = 4.26$ Å for the face-centered cubic TiN, which agrees with previous results using sputtering[17,18,20] and first-principles calculations.[28] These data show that bulk TiN grown by plasma enhanced ALD is preferentially (200)-oriented on Si (111) substrates. More material studies with synchrotron X-ray sources could help to understand the structure and ordering of ultra-thin films.

The chemical composition of TiN is discerned by X-ray Photoelectron Spectroscopy (XPS). We find a Ti:N stoichiometric ratio of 0.96 ± 0.04, determined by comparing the Ti $2p$ and N $1s$ peak areas with binding energies of 454.9 eV and 397.2 eV, respectively. In conjunction with XPS, we use secondary ion mass spectroscopy (performed by EAG Laboratories, Inc.) to quantify various impurities. The concentrations of H, C, and O are observed to be approximately 2%, 3%, and 1%, respectively, throughout the bulk TiN (Fig. S2).

Since oxygen is known to affect the properties of TiN, we characterize oxide growth on the film surface by XPS measurements. Ti $2p$ spectra from the surface indicate the presence of TiO_2 by the $2p_{3/2}$ peak at 458.6 eV [Fig. 1(c)]. The higher binding energy ($2p_{1/2}$) peaks are expected from spin-orbit coupling. Near the TiN surface, we find a thin intermediate TiO_xN_y transition layer.[22,29] The peak intensity of TiO_2 increases with aging, and we attribute this to a slow growth of a 5–8 nm thick oxide layer over a time scale of months. In addition, Ar^+ milling reveals that the TiO_xN_y transition layer persists and is between TiO_2 and bulk TiN. The presence and growth of an oxide layer, initiated by forming titanium oxynitride readily in atmosphere, are consistent with previous TiN film oxidation studies.[22,30] Since an amorphous oxide layer can act as a lossy dielectric, all resonators in this work are grown, patterned, and mounted inside a dilution refrigerator within three days to minimize

the time each film was exposed to an oxygen rich environment.

To verify that these films are low-loss at microwave frequencies, we pattern each film with a series of lumped element microwave resonators. Our design has an explicit capacitor and a meandering inductor to ground, as shown in Fig. 2(a). Each chip contains eight to ten resonators which are separated from a microwave feedline whose gap and pin width are carefully adjusted to match the 50 Ω impedance of the printed circuit board (PCB) and amplifier chain. On a single chip, all resonators are designed with equal capacitance C to ground. As a consequence, the resonance frequency f_0 is varied by adjusting the length of the inductor, while keeping the width constant at $w = 3\ \mu$m.

We measure resonators that vary in thickness from 8.9 nm to 109 nm and study the effect of the film thickness on the internal quality factor (see Fig. S3 for the measurement setup). A typical normalized transmission spectrum at a low average photon number ($n_{\mathrm{ph}} \approx 3$) of a resonator ($t = 109$ nm) is shown in the inset of Fig. 2(b). At the resonance frequency, we observe a dip in magnitude, which is captured well by

$$S_{21}^{-1} = 1 + \frac{Q_i}{Q_c^*} e^{i\phi} \frac{1}{1 + 2iQ_i(f - f_0)/f_0}, \tag{1}$$

where Q_c^* is the effective coupling quality factor and ϕ is the rotation in the complex S_{21}^{-1} plane due to impedance mismatches between the resonator and the feed line.[31] It is important to take this into account, especially for thin films ($t = 8.9$, 14.2 nm) where the high KI makes it difficult to avoid impedance mismatches between the feed line and PCB. Further investigation shows that Q_i increases at higher microwave power [Fig. 2(b)] and eventually saturates at $Q_{i,\mathrm{max}}$ for $n_{\mathrm{ph}} \gg 10^5$. This increase and saturation of Q_i are well described by a power dependent saturation mechanism,[32,33] which likely originates from two-level systems on the surface of TiN or Si.[19]

We now repeat the measurements from Fig. 2(b) for four film thicknesses between $t = 8.9$ and 109 nm and visualize the results in Fig. 2(c), where we plot Q_i of four separate chips grouped by film thickness. All resonators show high internal quality factors exceeding 1×10^5. In particular, the highest Q_i values are obtained with the $t = 49.8$ nm sample, for which seven of ten resonators have $Q_i(n_{\mathrm{ph}} = 1) > 10^6$. Since all resonators, except for those patterned on the thinnest film, show an increase in Q_i with incident microwave power, Q_i is most likely limited by two-level systems at $T = 20$ mK and $n_{\mathrm{ph}} = 1$. In contrast, resonators on the thinnest film ($t = 8.9$ nm) do not show this characteristic increase with power. Additionally, as the temperature is increased towards T_c, the Q_i of the thinnest resonators deviates significantly from a model derived from BCS theory (Fig. S4). This suggests that Q_i is limited by suppressed superconductivity instead of two-level systems. Nevertheless, these resonators still have high quality factors of $Q_i(n_{\mathrm{ph}} = 1) \approx 1 \times 10^5$.

In order to use these resonators in cavity QED experiments,[34] a high characteristic impedance Z is desirable since it can considerably enhance the coupling strength g. Since g is linearly proportional to the amplitude of zero-point fluctuations,[7] g scales as $f_0\sqrt{Z}$ (see supplementary material). We maximize the impedance of our lumped element resonator design by removing any explicit capacitor and making the resonator a meandering wire of width w and length ℓ, as shown in Fig. 3(a). For this design, the stray capacitance scales with the perimeter rather than the area of the resonator such that the resonance frequency $f_0 \propto (w/\ell^3)^{\frac{1}{4}}$ and impedance $Z \propto (\ell/w^3)^{\frac{1}{4}}$. From this, we expect an increased impedance as we decrease w from 2 μm to 75 nm, while keeping ℓ approximately constant.

Figure 3(b) shows the impedance and measured Q_i as a function of inductor wire width w for film thickness $t = 8.9$ (red) and 14.2 nm (blue). The maximum impedance of $Z = 28$ kΩ is achieved for the thinnest film and narrowest inductor, and since the electric dipole coupling strength in a hybrid system scales as $f_0\sqrt{Z}$, this would result in a coupling enhancement of $\sqrt{Z/50\,\Omega} \approx 24$ times. Even for the thickest film and widest wire, the impedance $Z = 1.76$ kΩ is more than 35 times larger than a conventional 50 Ω microwave resonator. For both films, we observe no strong dependence

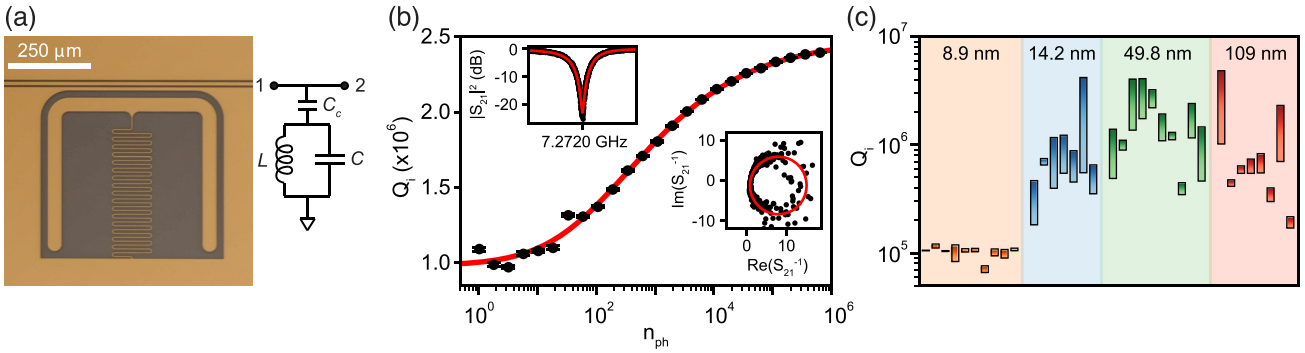

FIG. 2. Microwave characterization of high quality factor resonators. (a) Optical micrograph of a typical resonator ($t = 49.8$ nm) used in this work, which can be described by the circuit model shown on the right. We measure transmission from port 1 to port 2. (b) Power dependence of the internal quality factor for a resonator patterned on a 109 nm thick TiN film at $T = 20$ mK. The solid red line is a fit to a two-level system model that includes saturation at low and high powers. Insets show the lineshape (log magnitude, top left and inverse real and imaginary, lower right) at an average photon number $n_{\mathrm{ph}} \approx 3$. For this resonator $Q_c^* = 0.74 \times 10^5$. (c) Internal quality factors of all resonators in this study, grouped by film thickness. For a single film thickness, each resonator's internal quality factor increases with power, visualized as a bar. The bottom of each bar corresponds to single photon Q_i, whereas the top corresponds to the high power saturated Q_i or the Q_i just below bifurcation (if bifurcation was observed). The average Q_c^* of these resonators ranges from 1.1×10^5 ($t = 109$ nm) to 9.4×10^5 ($t = 14.2$ nm).

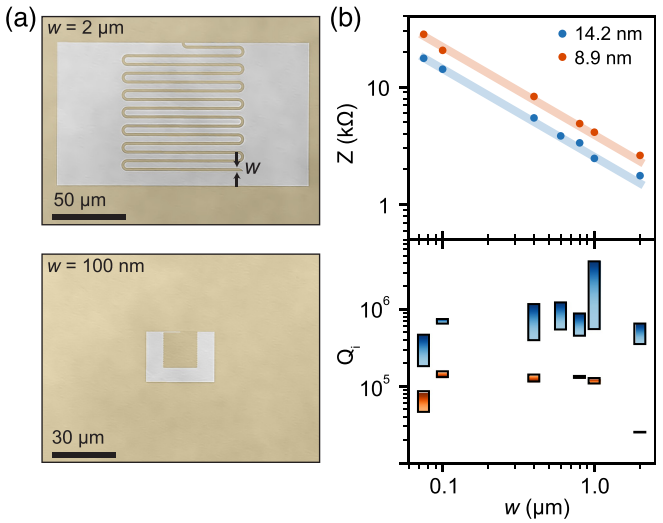

FIG. 3. High Q, high impedance resonators. (a) Optical micrographs of high impedance TiN (false-colored yellow) microwave resonators with inductor wire width $w = 2\,\mu$m (top) and $w = 100$ nm (bottom). Note the different scale bars. (b) Internal quality factor (top) at 20 mK and characteristic impedance (bottom) of the resonator designs shown in (a) as a function of w. Resonators are fabricated on TiN films $t = 8.9$ nm thick (red) and $t = 14.2$ nm thick (blue). Z is estimated from $2\pi f_0(w) L_\square \ell / w$, where both $L_\square$ (see Table I) and $f_0(w)$ were determined experimentally. The solid lines are a guide to the eye showing a $w^{-\frac{3}{4}}$ dependence as predicted from the main text.

of Q_i on w down to 75 nm, showing that we are able to produce high impedance resonators without having to sacrifice Q_i.

In conclusion, ALD grown TiN offers high quality films that can be used in detectors, hybrid systems, and protected qubits. Microwave resonators fabricated on films of thickness $t \geq 14.2$ nm showed internal quality factors exceeding 2×10^5 at single photon powers, whereas a reduced Q_i was observed for the thinnest film. On the thinnest film, a modified lumped element resonator design with no explicit capacitor and footprint of only $8 \times 8\ \mu\text{m}^2$ achieved impedances up to 28 kΩ. Moreover, we found no dependence of Q_i on the impedance down to $w = 75$ nm. Future work includes fabrication of high impedance resonators on different high KI films, such as NbN or NbTiN, and studying even narrower inductor wires down to $w = 10$ nm, where an increased phase slip rate may affect cavity quality factors and be an interesting platform for studying the breakdown of superconductivity.[35] In this regime, high KI materials can also be used in phase slip junctions.[36,37]

See supplementary material for a description of the experimental setup and additional DC and microwave film characterization.

The authors would like to thank S. Chakram for help with initial resonator measurements and A. S. Filatov for assistance with XPS studies. The authors would also like to thank P. Duda, A. Mukhortova, and A. Dixit for supporting device fabrication. We acknowledge useful discussions with Y. Lu, R. Naik, S. Hruszkewycz, and Q. Y. Tang. We thank J. Jureller for assistance with MRSEC facilities. This work was supported by the Army Research Office under Grant No. W911NF-17-C-0024. This work was partially supported by MRSEC (NSF DMR-1420709). Devices were fabricated in the Pritzker Nanofabrication Facility of the Institute for Molecular Engineering at the University of Chicago, which receives support from the Soft and Hybrid Nanotechnology Experimental (SHyNE) Resource (NSF ECCS-1542205), a node of the National Science Foundation's National Nanotechnology Coordinated Infrastructure. The work at Argonne National Lab (sample characterization) was supported by the U.S. Department of Energy, Office of Science, Basic Energy Sciences, Materials Science and Engineering Division. The use of the Center for Nanoscale Materials, an Office of Science user facility, was supported by the U.S. Department of Energy, Office of Science, Office of Basic Energy Sciences, under Contract No. DE-AC02-06CH11357.

[1]P. K. Day, H. G. LeDuc, B. A. Mazin, A. Vayonakis, and J. Zmuidzinas, Nature **425**, 817 EP (2003).
[2]G. Che, S. Gordon, P. Day, C. Groppi, R. Jackson, H. Mani, P. Mauskopf, H. Surdi, G. Trichopoulos, and M. Underhill, preprint arXiv:1710.11335 (2017).
[3]A. Kher, P. K. Day, B. H. Eom, J. Zmuidzinas, and H. G. Leduc, J. Low Temp. Phys. **184**, 480 (2016).
[4]B. Ho Eom, P. K. Day, H. G. LeDuc, and J. Zmuidzinas, Nat. Phys. **8**, 623 EP (2012).
[5]N. Samkharadze, G. Zheng, N. Kalhor, D. Brousse, A. Sammak, U. C. Mendes, A. Blais, G. Scappucci, and L. M. K. Vandersypen, Science **359**, 1123 (2018).
[6]A. J. Landig, J. V. Koski, P. Scarlino, U. C. Mendes, A. Blais, C. Reichl, W. Wegscheider, A. Wallraff, K. Ensslin, and T. Ihn, Nature **560**, 179 (2018).
[7]N. Samkharadze, A. Bruno, P. Scarlino, G. Zheng, D. P. DiVincenzo, L. DiCarlo, and L. M. K. Vandersypen, Phys. Rev. Appl. **5**, 044004 (2016).
[8]A. J. Kerman, Phys. Rev. Lett. **104**, 027002 (2010).
[9]M. T. Bell, J. Paramanandam, L. B. Ioffe, and M. E. Gershenson, Phys. Rev. Lett. **112**, 167001 (2014).
[10]J. M. Dempster, B. Fu, D. G. Ferguson, D. I. Schuster, and J. Koch, Phys. Rev. B **90**, 094518 (2014).
[11]N. Earnest, S. Chakram, Y. Lu, N. Irons, R. K. Naik, N. Leung, L. Ocola, D. A. Czaplewski, B. Baker, J. Lawrence, J. Koch, and D. I. Schuster, Phys. Rev. Lett. **120**, 150504 (2018).
[12]Y.-H. Lin, L. B. Nguyen, N. Grabon, J. San Miguel, N. Pankratova, and V. E. Manucharyan, Phys. Rev. Lett. **120**, 150503 (2018).
[13]I. M. Pop, K. Geerlings, G. Catelani, R. J. Schoelkopf, L. I. Glazman, and M. H. Devoret, Nature **508**, 369 (2014).
[14]T. M. Hazard, A. D. P. A. Gyenis, A. T. Asfaw, S. A. Lyon, A. Blais, and A. A. Houck, preprint arXiv:1805.00938 (2018).
[15]J. B. Chang, M. R. Vissers, A. D. Córcoles, M. Sandberg, J. Gao, D. W. Abraham, J. M. Chow, J. M. Gambetta, M. Beth Rothwell, G. A. Keefe, M. Steffen, and D. P. Pappas, Appl. Phys. Lett. **103**, 012602 (2013).
[16]M. Sandberg, M. R. Vissers, T. A. Ohki, J. Gao, J. Aumentado, M. Weides, and D. P. Pappas, Appl. Phys. Lett. **102**, 072601 (2013).
[17]M. R. Vissers, J. Gao, D. S. Wisbey, D. A. Hite, C. C. Tsuei, A. D. Corcoles, M. Steffen, and D. P. Pappas, Appl. Phys. Lett. **97**, 232509 (2010).
[18]S. Ohya, B. Chiaro, A. Megrant, C. Neill, R. Barends, Y. Chen, J. Kelly, D. Low, J. Mutus, P. J. J. O'Malley, P. Roushan, D. Sank, A. Vainsencher, J. Wenner, T. C. White, Y. Yin, B. D. Schultz, C. J. Palmstrøm, B. A. Mazin, A. N. Cleland, and J. M. Martinis, Supercond. Sci. Technol. **27**, 015009 (2014).
[19]M. Sandberg, M. R. Vissers, J. S. Kline, M. Weides, J. Gao, D. S. Wisbey, and D. P. Pappas, Appl. Phys. Lett. **100**, 262605 (2012).
[20]H. M. I. Jaim, J. A. Aguilar, B. Sarabi, Y. J. Rosen, A. N. Ramanayaka, E. H. Lock, C. J. K. Richardson, and K. D. Osborn, IEEE Trans. Appl. Supercond. **25**, 1 (2015).
[21]P. C. J. J. Coumou, M. R. Zuiddam, E. F. C. Driessen, P. J. de Visser, J. J. A. Baselmans, and T. M. Klapwijk, IEEE Trans. Appl. Supercond. **23**, 7500404 (2013).
[22]M. Nahar, N. Rocklein, M. Andreas, G. Funston, and D. Goodner, J. Vac. Sci. Technol., A **35**, 01B144 (2017).
[23]E. F. C. Driessen, P. C. J. J. Coumou, R. R. Tromp, P. J. de Visser, and T. M. Klapwijk, Phys. Rev. Lett. **109**, 107003 (2012).

[24]Y. Ivry, C.-S. Kim, A. E. Dane, D. De Fazio, A. N. McCaughan, K. A. Sunter, Q. Zhao, and K. K. Berggren, Phys. Rev. B **90**, 214515 (2014).
[25]P. C. J. J. Coumou, E. F. C. Driessen, J. Bueno, C. Chapelier, and T. M. Klapwijk, Phys. Rev. B **88**, 180505 (2013).
[26]W. Escoffier, C. Chapelier, N. Hadacek, and J.-C. Villégier, Phys. Rev. Lett. **93**, 217005 (2004).
[27]U. S. Pracht, M. Scheffler, M. Dressel, D. F. Kalok, C. Strunk, and T. I. Baturina, Phys. Rev. B **86**, 184503 (2012).
[28]S. Hao, B. Delley, and C. Stampfl, Phys. Rev. B **74**, 035402 (2006).
[29]N. Saha and H. Tompkins, J. Appl. Phys. **72**, 3072 (1992).
[30]S. Logothetidis, E. Meletis, G. Stergioudis, and A. Adjaottor, Thin Solid Films **338**, 304 (1999).
[31]A. Megrant, C. Neill, R. Barends, B. Chiaro, Y. Chen, L. Feigl, J. Kelly, E. Lucero, M. Mariantoni, P. J. J. O'Malley, D. Sank, A. Vainsencher, J. Wenner, T. C. White, Y. Yin, J. Zhao, C. J. Palmstrøm, J. M. Martinis, and A. N. Cleland, Appl. Phys. Lett. **100**, 113510 (2012).
[32]H. Wang, M. Hofheinz, J. Wenner, M. Ansmann, R. C. Bialczak, M. Lenander, E. Lucero, M. Neeley, A. D. O'Connell, D. Sank, M. Weides, A. N. Cleland, and J. M. Martinis, Appl. Phys. Lett. **95**, 233508 (2009).
[33]J. M. Sage, V. Bolkhovsky, W. D. Oliver, B. Turek, and P. B. Welander, J. Appl. Phys. **109**, 063915 (2011).
[34]Z.-L. Xiang, S. Ashhab, J. Q. You, and F. Nori, Rev. Mod. Phys. **85**, 623 (2013).
[35]R. Kuzmin, R. Mencia, N. Grabon, N. Mehta, Y.-H. Lin, and V. E. Manucharyan, preprint arXiv:1805.07379 (2018).
[36]J. E. Mooij and Y. V. Nazarov, Nat. Phys. **2**, 169 (2006).
[37]S. E. D. Graaf, S. T. Skacel, R. Shaikhaidarov, H. Rotzinger, and S. Linzen, Nat. Phys. **14**, 590 (2018).